

Contents lists available atScienceDirect

Materials Chemistry and Physics

journal homepage: www.elsevier.com/locate/matchemphys



Synergistic enhancement of CO₂ capture via amine decorated hierarchical MIL-101(Cr)/SBA-15 composites

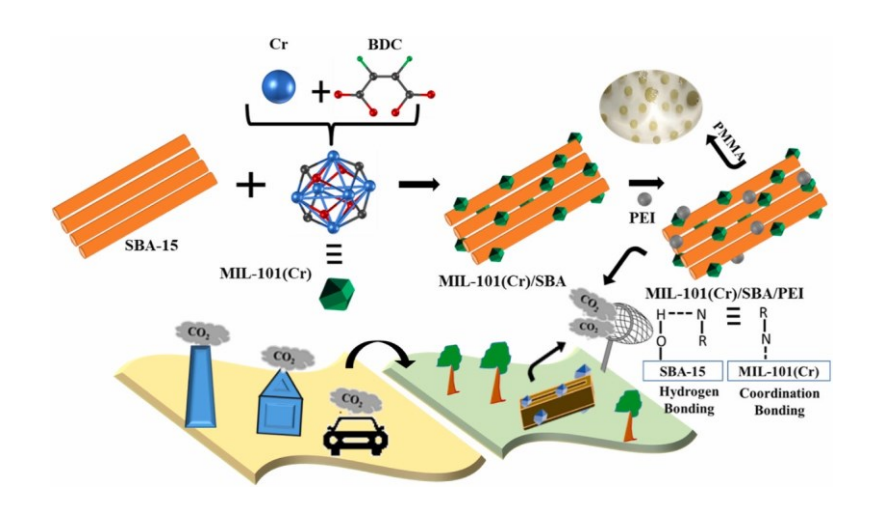


Debarati Mukherjee ^a, Saif Hassan ^b, Juvairia Shajahan ^a, Aleksandrs Prokofjevs ^a, Debasish Kuila ^{a,*}

- ^a Department of Chemistry, North Carolina Agricultural and Technical State University, Greensboro, NC, USA
- b Department of Chemical, Biological and Bioengineering, North Carolina Agricultural and Technical State University, Greensboro, NC, USA

HIGHLIGHTS

- PEI incorporated MIL-101(Cr)/SBA-15 composites for CO₂ capture.
- Increased mesoporosity upon SBA-15 incorporation in the MOF enhance CO₂ adsorption
- MIL-101(Cr)/SBA/PEI-25 adsorbed 3.2 mmol/g of pure and 1.6 mmol/g of 400 ppm CO₂.
- Adsorption was exothermic in nature with Q_{ist} ranging from 52 to 45 kJ/mol.
- Efficient composite regeneration at 65 °C for 120 min under N₂ atmosphere.



ARTICLEINFO

Keywords: MIL-101(Cr) SBA-15 Carbon capture Hierarchical

ABSTRACT

Synthesis of amine incorporated hierarchical metal organic framework (MOF) MIL-101(Cr)/SBA-15, meso/ micro-porous composites, with tailored properties for CO₂ capture is reported. The synthesized composites were characterized in terms of their crystallinity, morphology, functional groups, and textural properties. Isothermal adsorption of CO₂ from concentrated sites as well as ambient conditions were evaluated by gravimetric and volumetric measurements. The optimized composite i.e., MIL-101(Cr)/SBA-15/PEI-25 showed improved pseudo- equilibrium adsorption capacity of 3.2 mmol/g at 303 K and 1 bar, compared to nascent SBA-15 (0.8 mmol/g) and the MOF, i.e., MIL-101(Cr) (1.3 mmol/g). Such adsorption performance can be attributed to the basic sites of the impregnated polyethyleneimine (PEI), unsaturated Cr(III) metal sites, and the hierarchical pore structure of the composite which imparts chemical as well physical adsorption forces towards CO₂ uptake. Interestingly, lower amine loading of 25 wt% in the composite resulted in facile CO₂ desorption at much lower temperature of

* Corresponding author.

GRAPHICALABSTRACT

E-mail addresses: mdebarati89@gmail.com (D. Mukherjee), saifnabilhassan31@gmail.com (S. Hassan), jshajahan@aggies.ncat.edu (J. Shajahan), aprokofjevs@ ncat.edu (A.

Prokofjevs), dkuila@ncat.edu (D. Kuila). https://doi.org/10.1016/j.matchemphys.2024.129533

Received 30 January 2024; Received in revised form 22 May 2024; Accepted 30 May 2024 Available online 31 May 2024

0254-0584/© 2024 Published by Elsevier B.V.

65 °C. This guaranteed energy-efficiency and good reusability of the composite, after ten cycles, are evident from their structural and morphological studies.

1. Introduction

Continuous release of carbon dioxide (CO_2) from various sources, such as consumption of fossil fuels, increased transportation, population growth, etc., is one of the dominant factors for global warming. This has prompted academic researchers as well as industry to focus on environmentally sustainable solutions for carbon capture to attain carbon neutrality [1]. Different technologies are being developed to reduce the carbon footprint, slowing the release of carbon dioxide into the atmosphere and carbon capture and sequestration (CCS) from the environment [2,3]. Adsorption emerges as a promising technology compared to other CO_2 capture processes due to their ease of operation and energy efficiency (Huck et al., 2014; [4,5]). More significantly, cost-effective, non-toxic, multi-functional materials with high CO_2 capture efficiency are currently being developed to create a clean and green environment in the future.

Currently, activated carbon [6], carbon nanotubes [7], zeolites [8], alkalinebased sorbents [9], polymers [10], mesoporous silica (Li et al., 2015), and metal-organic frameworks (MOFs) [11] are being investigated for CO₂ capture applications. Among the reported porous adsorbents, MOFs, an organicinorganic hybrid, have inculcated a special interest due to their wide applications ranging from separation, drug delivery, sensors, fuel cell, catalysis, gas adsorption, etc. [12–14]. The unsaturated metal center in MOFs, along with their high surface area, crystallinity, high porosity, and tunable pore size, make them highly promising candidates for CO₂ capture [15]. In 2005, Ferey et al. synthesized MIL-101 (Cr) via hydrothermal synthesis. It possessed high crystallinity with pentagonal and hexagonal windows in the range from 20 to 45 Å [16]. This MIL-101 MOF was found to be stable and resistant to moisture and heat. However, microporous MOFs often experience resistance to diffusion and mass transfer (Shen et al., 2018). This can be circumvented by introducing macro or mesopores within the MOF framework via in-situ or postsynthetic modifications with polymers, graphene oxide, mesoporous materials, etc. [17,18]. MCM-41 incorporated Cu(BDC), synthesized via microwave route, resulted in enhanced CO2 adsorption and selectivity compared to the nascent counterparts [19]. Among the mesoporous materials, SBA-15 is a promising candidate for use in CO₂ capture applications due to its impressive thermal stability, high-temperature resistance, and ease of surface functionalization [20]. For instance, the structural and morphological characterizations of the Mg-MOF-74@SBA-15 composite showed growth of the MOF nanoparticles inside the mesopores of SBA-15 [21]. However, the CO₂ adsorption of the composite was lower than the MOF. Chen et al. [22] synthesized a hierarchical SBA-15@HKUST-1 composite, via a solvothermal approach, for CO₂ adsorption. The structure-directing property of SBA-15 led to alteration in the morphology of HKUST-1 from octahedron to flowerlike composite with a hundred-fold reduction in the particle size (10–15 μm to 100-200 nm). The composite showed enhanced CO₂ uptake as compared to HKUST-1 or SBA-15 due to the reduction in diffusion path and mass transfer resistance. However, till date, little research has been reported on micromesoporous materials for gas adsorption.

Herein, we present the controllable synthesis of hierarchichal mesoporous/micrporous MIL-101(Cr)/SBA-15 composite. The effect of the morphological tuning due to the synergistic effect of the MOF and SBA- 15 on CO₂ adsorption and desorption has not been studied before. The ordered mesoporous structure of SBA-15 controlled the growth of MIL- 101(Cr) crystals accelerating CO2 diffusion. In previous studies, impregnating amines such as polyethyleneimine (PEI) into MOF framework has emerged as an efficient pathway for improving CO₂ capture performance due to the -NH₂-CO₂ interactions. When PEI is uniformly distributed on the inner surface of MOF composite without causing pore blockage, it is anticipated that the synergistic interaction between them will enhance the performance of CO₂ capture [23]. In the present study, to improve the CO2 uptake, the developed MIL-101 (Cr)/SBA-15 composite has been modified with PEI to increase the basic sites facilitating the chemisorption of CO₂. The direct air capture efficiency of the optimized composite was also assessed using 400 ppm of CO₂ (balance nitrogen) in the adsorbate stream. However, the CO2 desorption of amine impregnated MOFs usually occurs at higher temperature rendering the process

to be energy-intensive [15,23,24]. In order to overcome this limitation, we have tried to modify the pore structure of the MOF composite since the presence of large pores is expected to facilitate CO_2 desorption as reported by Ref. [25]. This implies the significance of incorporating mesoporous SBA-15 in MOF framework. The adsorption-desorption using the optimized composite was performed under temperature swing mode. The hierarchical structure is expected to exhibit CO_2 desorption at lower temperature as compared to the nascent MOF, which has been demonstrated experimentally.

Additionally, in order to assess the usability of the adsorbent usage in large-scale, an approach to pelletize the optimized powder composite without significant change in the adsorption efficiency was underaken. The pellets are reported to reduce the pressure drop and non-uniform gas flow compared to powders in large-scale adsorption columns [26]. The pelletization involved the use of poly (methyl methacrylate) (PMMA) as a binder [26]. PMMA has a good affinity for $\rm CO_2$ sorption and diffusion [27], resulting in minimum alteration of the adsorption properties of the composite. Overall, our work demonstrates an approach for design of porous amine modified MOF based composite, which is expected to contribute to the goal of eliminating gaseous pollutants to achieve a clean green environment.

2. Experimental

2.1. Materials

All the chemicals used in the synthesis of the materials, including chromium nitrate (Cr(NO₃)₃·9H₂O), terephthalic acid (H₂BDC), SBA-15 (<150 μ m particle size), polyethyleneimine (PEI) (molecular weight- 800 g/mol), poly (methyl methacrylate) (PMMA), methanol N, N- dimethylformamide (DMF), acetone were purchased from Sigma Aldrich and Fisher Scientific and used without any further purification.

2.2. Synthesis

2.2.1. Synthesis of MIL-101(Cr)

MIL-101(Cr) was synthesized following the hydrothermal route devoid of hydrofluoric acid with some minor modifications [28]. Typically, $Cr(NO_3)_3.9H_2O$ (2.0 g) and terephthalic acid (0.83 g) were thoroughly mixed with deionized water (20 mL) via ultrasonication for 2 h. The resulting blue-colored solution was subjected to hydrothermal treatment at 218 °C for 18 h using a Teflon-lined stainless-steel autoclave. The resulting solid precipitate was separated using centrifugation and washed with water and methanol. The washed residue was dispersed in DMF, sonicated for 1 h, and stirred at 80 °C for 24 h for complete removal of the unreacted terephthalic acid. Subsequently, the MOF particles were washed three times each using methanol and acetone, followed by overnight air drying at 85 °C and vacuum drying at 120 °C for 24 h. The synthesized MOF resulted in a higher surface area as compared to the reported data, probably due to the alteration in the washing and drying protocol, which led to the complete removal of solvents.

2.2.2. Synthesis of MIL-101(Cr)/SBA-15

The mesoporous silica incorporated MOF composite was synthesized following the aforementioned similar protocol as MIL-101(Cr). SBA-15 (10 wt% with respect to the metal precursor) was added to the solution of $Cr(NO_3)_3$ -9H₂O and terephthalic acid and subjected to hydrothermal treatment [22]. The resultant washed and dried MIL-101(Cr)/SBA-15 composite was stored in a vacuum desiccator for further use.

2.2.3. Synthesis of amine impregnated MIL-101(Cr)/SBA-15

The MIL-101(Cr)/SBA-15 composite was modified using PEI ranging from 10 to 50 wt%. The composite was activated at 120 °C for 24 h prior to amine functionalization. PEI was first dissolved in methanol, followed by the addition of the composite. The resulting mixture was sonicated for 24 h and stirred overnight to form a homogeneous suspension [2]. Subsequently, methanol was removed by air drying at 65 °C followed by vacuum drying at 40 °C for 24 h. The samples were labeled as MIL-101 (Cr)/SBA-15/PEI-x, where x refers to the amount of PEI added (x = 10, 20, 25, 30, 50).

2.2.4. Synthesis of spherical shaped MIL-101(Cr)/SBA-15/PEI

The synthesis of shaped MIL-101(Cr)/SBA-15/PEI using PMMA as a binder was performed via drop casting and phase inversion [26,29]. Considering 1 g batch, PMMA (100 mg) was added to CHCl $_3$ (3 ml), accompanied by continuous stirring to form a clear solution. The composite, MIL-101(Cr)/SBA-15/PEI (900 mg), was dispersed in the PMMA solution by ultrasonication for 3 h, followed by overnight stirring at 60 °C. The solution was dropped vertically into a nonsolvent bath of distilled water using a 19 gauge needle attached to a 5 ml syringe. The obtained beads were immersed in the nonsolvent water bath for 30 min, followed by replacing them with fresh water for another 30 min. Finally, the PMMA-incorporated composite beads were dried at 65 °C overnight in a regular oven. 2.3. Characterizations

The as-synthesized materials were characterized using powder X-ray diffraction (XRD; Bruker AXS). The analysis was conducted using a Cu Kα1 radiation ($\lambda = 1.5406$ Å) by varying 20 from 10 to 80° with a step interval of 0.02°. The functional groups were analyzed using Fourier Transform Infrared Spectroscopy (FTIR; Shimadzu IR Prestige-21 equipped with mercury cadmiumtelluride detector) within the wavenumber range 400-4000 cm⁻¹. X-ray photoelectron spectroscopy (XPS; Escalab Xi + -, Thermo Scientific) was used to assess the binding energy of the samples. The Brunauer- Emmett- Teller (BET) surface area and porosity (including Barrett-Joyner-Halenda (BJH) desorption pore size and pore volume) of the samples were estimated from the N_2 adsorption – desorption isotherms (3-flex Micromeritics ASAP 2020). The samples were pretreated for 6 h under vacuum at 120 °C for complete removal of moisture and other surface impurities. The particle size and morphology were analyzed using Field Emission Scanning Electron Microscopy (FESEM; JEOL JSM-IT800) and Field Emission Transmission Electron Microscopy (FETEM; Thermo Fischer Talos F200X).

2.4. CO2 adsorption

2.4.1. TGA and BET experiments

The gravimetric and volumetric CO_2 adsorption capacity of the samples were estimated using thermogravimetric analysis (TGA/Differential scanning Calorimetry DSC; TA instruments) and BET physisorption, respectively. For TGA analysis, the samples were subjected to N_2 flow for 180 min for activation, followed by CO_2 (pure and 400 ppm) adsorption at 30, 40, and 50 °C with a flow rate of 90 ml/min. The adsorption equilibration was performed for 180 min. Desorption was conducted at 65 °C for 120 min under an N_2 atmosphere. The repeatability of the experiments have been demonstrated by performing the experiments in triplicate. This approach provides a visual representation of the variability in the data while emphasizing the central tendency captured by the mean measurement. In the case of BET analysis, 0.1 g of the samples were activated for 6 h at 120 °C. Adsorption of pure CO_2 was performed at three different temperatures, i.e., 30, 40, and 50 °C, for absolute pressure ranging from 0 to 760 mm Hg. The cell pressure was manually monitored.

Primarily, adsorption studies were performed using pure CO_2 to determine the efficiency of the synthesized materials. The optimized adsorbent was further investigated for direct air capture, i.e., adsorption of 400 ppm CO_2 at ambient conditions (1 bar and 30 °C).

In the case of adsorption-based separation of CO_2 from gas mixtures such as N_2 , the selectivity of adsorption also emerges as a pivotal determinant of separation efficacy beyond just focusing on the adsorption capacity. In the current study, Ideal Adsorbed Solution Theory (IAST) was used to calculate the CO_2/N_2 selectivity (S) (Eqn (1)) [30].

$$\underline{SS}_{\underline{1}2} = \frac{xy_{\underline{1}1}}{x}y_{\underline{2}2} \tag{1}$$

Here x and y represents mole fractions of gases 1 (CO2) and 2 (N2) in the adsorbed phase and gas phase, respectively.

2.4.2. Adsorption isotherm and kinetics

Temperature and contact time are the primary factors to affect gas/ liquid adsorption. The relationship between the adsorbate, i.e., CO_2 in the gas phase, and that adsorbed on the adsorbent surface during dynamic equilibrium is represented by adsorption isotherm plots [31]. The amount of CO_2 (mg or mmol) adsorbed per unit mass (g) or surface area (m²) of the adsorbent represents the adsorption capacity (Q) of the adsorbent at the operating temperature and pressure. In the present study, the nature of adsorption was analyzed by fitting the obtained adsorption data points using Langmuir, Sips, and Toth adsorption isotherm (Eqns. (2)–(4)), which are widely used for gas adsorption studies.

$$Q_{\ell} = 1\underline{Q} + \underline{K}\underline{K}\underline{L}\underline{P}P \tag{2}$$

$$Q_{\mathcal{E}} = \underline{Q_m(\underline{b_A P})_{\underline{1}n\underline{1}}} \tag{3}$$

 $1 + (b_A P)_n$

$$Q_{e} = \frac{q}{n} \underline{1}^{n}$$

$$[1 + (b_{A}P)]$$

$$(4)$$

Where, Q_e (mmol/g) represents the equilibrium adsorption capacity, P is the gas phase adsorption pressure, Q_m (mmol/g) is the maximum adsorption capacity, K_L is the Langmuir adsorption equilibrium constant, n is the heterogeneity factor and b_A is the Toth and Sips adsorption isotherm constant.

The isosteric heat of adsorption (Q_{lst}) , which represents the adsorption enthalpy, signifies the extent of interaction between the adsorbent and adsorbate. Q_{lst} was calculated based on the Clausius – Clapeyron equation (Eqn. (5)). The dependency of the adsorption capacity with absolute pressure at three different temperatures (30, 40, 50 °C) was used to calculate Q_{lst} .

()()

In $P = -QR_{ist}R_1 + c$ (5) where T, P, R, and C represent the temperature,

pressure, universal gas constant, and integration constant, respectively,

The evaluation of the kinetics of CO₂ adsorption on the synthesized adsorbents is required to apprehend the overall mass transfer in the process. The time-dependent adsorption data obtained from TGA were fitted using the pseudo-second-order kinetic model (Eqn. (6)).

$$Q\underline{\mathbf{t}}_t = KQ\underline{\mathbf{1}}_{2e} + Q\underline{\mathbf{t}}_e \tag{6}$$

Where, Q_t (mmol/g) represents the adsorption capacity obtained at various time intervals (t), and K is the pseudo-second-order kinetic rate constant.

2.4.3. Reusability studies

The reusability of the optimized adsorbent was assessed in terms of their CO_2 adsorption capacity at 30 °C, 1 bar from three consecutive cycles of adsorption-desorption experiments. The desorption was performed at 65 °C, 1 bar for 120 min under an N_2 atmosphere. The reused adsorbent was characterized using FTIR and FESEM to analyze their structural and morphological integrity. **3. Results and discussions**

3.1. Materials characterization

The composites, its different components and the MOF were characterized using different techniques. The wide-angle XRD plot (Fig. 1a) shows the formation of crystalline material. The peak positions at $2\theta \equiv 5.92^\circ$, 9.03° , 9.62° , and 16.9° confirm MIL-101 (Cr) structure [28]. Upon incorporation of SBA-15, the peak positions remained the same, with a decrease in crystallinity due to the pore filling effect. The diffraction peaks corresponding

to SBA-15 were not detected in the spectra, probably due to its lower loading and improved dispersion in the MOF framework.

Fig. 1b represents the FTIR plot of the composites. MIL-101(Cr) shows a peak at 1411 cm⁻¹, indicating O–C–O symmetric stretch corresponding to the dicarboxylic acid linkers. The Cr–O vibration is demonstrated by the peak at 560 cm⁻¹[32]. MIL-101/SBA composites did not show any significant changes compared to the nascent MOF. This suggests that the MOF framework was retained even after SBA incorporation. The spherical composites, formed with PMMA as a binder, showed peaks at 1103 and 1152 cm⁻¹ that correspond to the C–H deformation of PMMA (Fig. S1) [33]. The other peaks remained unchanged as observed in the nascent MOF.

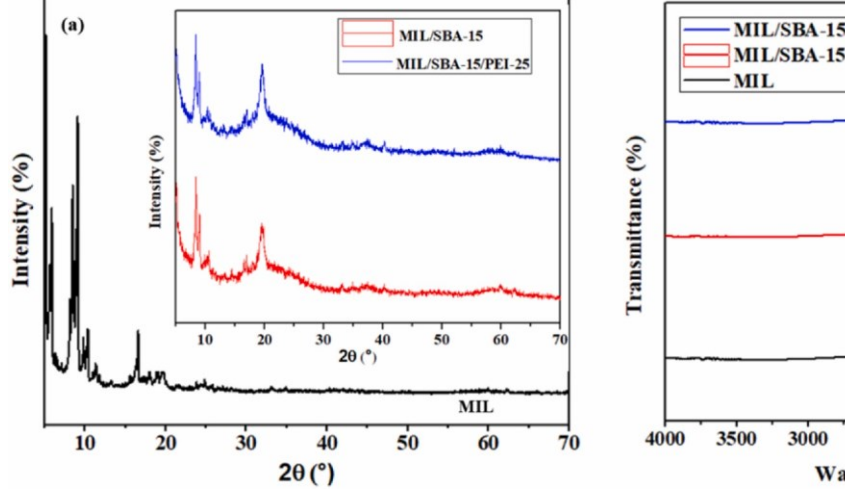
The XPS spectra of the synthesized materials are presented in Fig. 2. The surface scan (Fig. 2a) shows representative Cr 2p peaks for MIL-101 and its composites. Fig. 2b shows Cr 2p1/2 and Cr 2p3/2 peaks at 577.27 and 587.07 eV, confirming the formation of MIL-101(Cr) [34] and the existence of Cr in its +3 ±valence state. The incorporation of SBA-15 in the MOF framework led to the development of Si 2p characteristic peaks in the composites (Fig. 2a). The Cr 2p1/2 and Cr 2p3/2 peaks slightly shifted to higher binding energies, 577.36 and 587.17 eV, respectively. This may suggest alteration in the coordination environment of Cr(III) metal centers that may lead to a shift in the peak positions. The nitrogen wt.% of the amine impregnated composites (10, 20, 25, 30, 50) were determined from XPS surface scan and reported in Table S1.

The morphologies of the MOF and composites were also analyzed using FESEM and FETEM. Fig. 3a shows the uniform octahedral morphology of MIL-101(Cr). SBA-15 has smooth, elongated micron-sized rod-like morphology (Fig. 3b). Combination of these two materials results in roughness on the SBA-15 surface accompanied by folding and bending of the SBA channels due to growth of the MOF crystals on their surface (Fig. 3c). The morphology did not alter significantly upon impregnating PEI on the composite (Fig. 3d) and even

for the PMMA mixed particles (Fig. S1b). FESEM-EDS of all the amine modified MIL- 101/SBA-15 composites were conducted (Fig. S2) to determine the nitrogen wt.% (Table S1).

The morphology and particle size were further confirmed using FETEM (Fig. S3). The bright field images showed changes in the octahedral morphology of nascent MOF to cylindrical composites. MIL-101 had a particle size of ~200 nm (Fig. S3a). The growth of MOF crystals on SBA-15 resulted in a reduction of their particle size from a few microns (Fig. 3b) to the nanometer range (Fig. S3b).

The N₂ adsorption-desorption isotherms of the synthesized materials are presented in Fig. 4a. MIL-101(Cr) revealed a typical type I isotherm indicating the dominance of microporosity, whereas SBA-15 displayed type IV isotherm. SBA-15 decorated MIL-101(Cr) composites represented an amalgamation of both types I and type IV adsorption isotherms. This is a clear indication of the hierarchical structure, i.e., the presence of microporosity and mesoporosity of the composites. The BET surface area of MIL-101(Cr) was found to be 4943 m²/g. This is comparatively higher than the reported surface area of MIL-101(Cr) (~4230 m²/g) [2,35]. The surface area decreased upon the formation of the SBA composite, which was further reduced upon PEI incorporation. The pore size distribution (Fig. 4b) suggested the increased volume of mesopores in MIL-101(Cr)/SBA-15 as compared to nascent MIL-101 (Cr). Although the total pore volume of the nascent MOF is higher, the mesopore volume substantially increased from 0.65 in nascent MOF to 1.62 cm³/g in the MOF/SBA composite (Table 1). This facilitates mass transport of molecules, resulting in enhancement of the adsorption capacity [36]. In contrast, SBA-15 showed higher mesopore volume as compared to the composites, inferring the growth of MOF crystals on both the external surface as well as pores of SBA-15 [37]. The role of SBA-15 as a structure-directing agent during MIL-101(Cr) growth can be clearly inferred from the pore size distribution plots [37]. The detailed



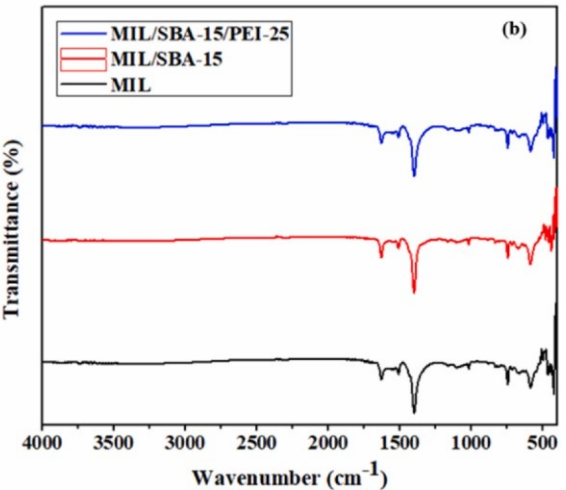


Fig. 1. (a) XRD; (b) FTIR of MIL-101(Cr), MIL-101(Cr)/SBA-15, MIL-101(Cr)/SBA-15/PEI-25.

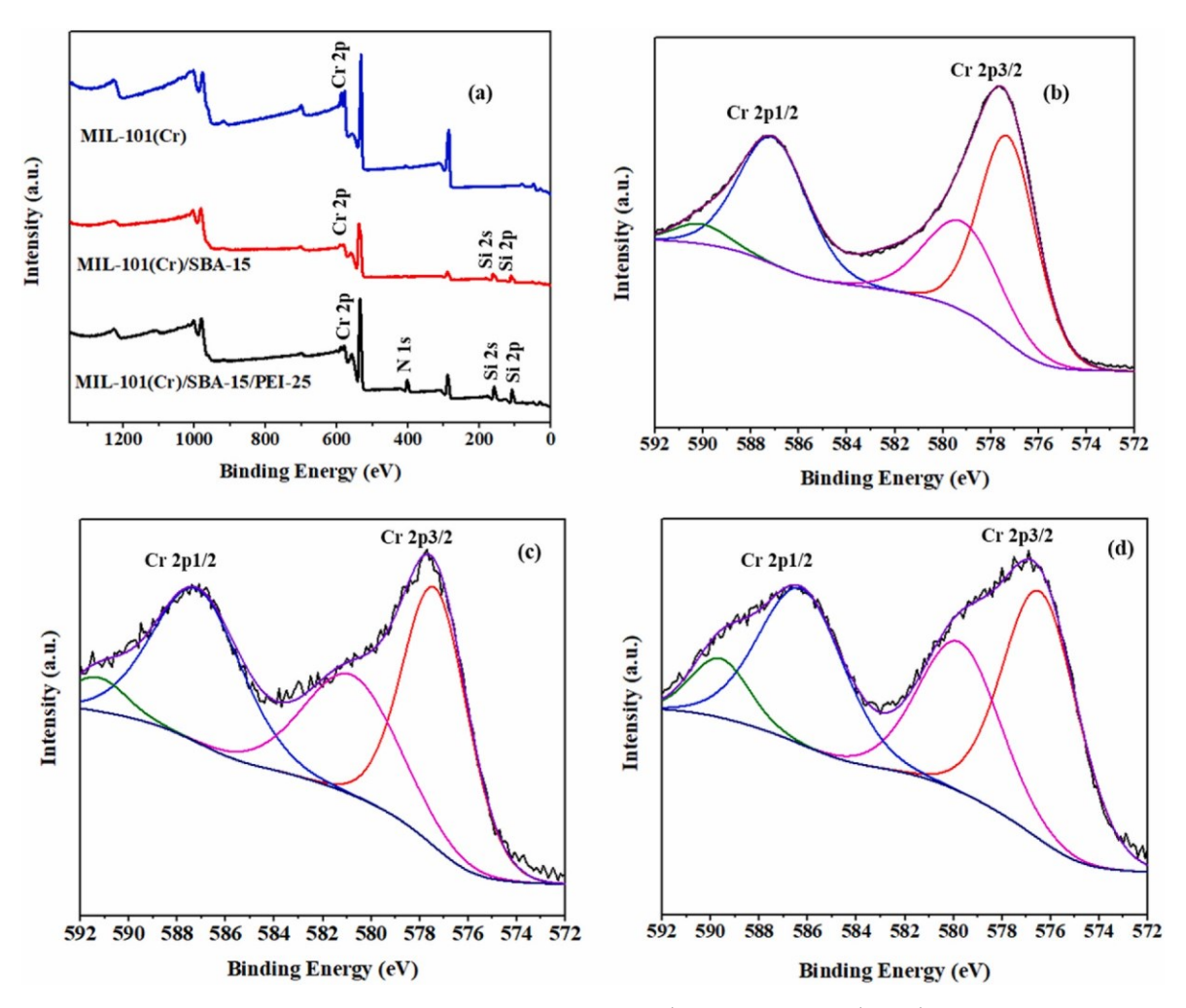


Fig. 2. (a) Surface XPS spectra and (b) Cr 2p core spectra of MIL-101(Cr), MIL-101(Cr)/SBA-15, and MIL-101(Cr)/SBA-15/PEI-25.

textural properties are shown in Table 1.

Based on the aforementioned structural and morphological characterizations, a plausible mechanism for the formation of MOF crystals on the surface of SBA-15 is proposed. The primary stages involved in the process are nucleation, growth, and attachment of the MOF crystals on the SBA-15 during the hydrothermal process under temperature and pressure. Upon dispersion of SBA-15 into the Cr+3 metal ion precursor, diffusion of the metal ions occurs into the mesopores of SBA-15, followed by coordination with the silanol groups on the surface. Subsequently, the reaction between Cr+3 metal ion and the BTC linker results in the formation of MOF nuclei in a controlled manner due to the silanol group containing SBA-15, which acts as nucleation sites. Finally, the growth and attachment of these MIL-101(Cr) crystals occur on the SBA-15 matrix [37] resulting in the composite formation.

3.2. CO2 adsorption

The pure CO_2 adsorption capacities of SBA-15, MIL-101(Cr), MIL-101(Cr)/SBA, and MIL/SBA/PEI-25 estimated by the gravimetric process at 30 °C and 1 bar are shown in Fig. 5a. The plot displays the effect of adsorption time on the pseudo-equilibrium adsorption capacity. SBA- 15 showed a steep increase in the adsorption capacity within 30 min, after which it became almost stable. This might be due to the presence of mesopores in SBA-15, which initially promotes adsorption, but after a certain time, becomes saturated with CO_2 molecules. In contrast, MIL and SBA decorated MIL composites displayed a gradual increase in CO_2 adsorption, and after 10 min, the capacity exceeded that of SBA-15 alone. The adsorption capacities of the materials as a function of pressure, estimated by the volumetric process, are presented in Fig. 5b.

Almost similar results were obtained with both volumetric and gravimetric methods. While SBA-15 showed an adsorption capacity of 0.8 mmol/g, consistent with reported data [22], the nascent MOF displayed a somewhat higher adsorption capacity of 1.3 mmol/g as compared to that reported in the literature [15].

The adsorption efficiency of MIL-101(Cr)/SBA (2.1 mmol/g) was significantly enhanced compared to the nascent MOF (1.3 mmol/g) or SBA-15 (0.8 mmol/g). The pore size distribution reveals increased mesopore volume and pore diameter of SBA-15 compared to MIL-101. Hence, when SBA-15 was incorporated in the MOF framework, the enhanced mesoporosity resulted in more gas adsorption sites. This is indeed novel for this mixed composite. Additionally, it improved CO₂ diffusion and hence enhanced mass transfer from the gas phase to the solid phase. We believe that the synergistic interplay between MIL-101 (Cr) and SBA-15 was responsible for the improved adsorption [38]. The adsorption further increased with amine incorporation via an acid-base reaction of CO₂ with the modified composite. At the early stage of PEI loading from 10 to 25 wt%, the increased chemisorption of CO₂ resulted in increased CO₂ adsorption (Fig. S4). The low molecular weight of PEI facilitates its uniform dispersion within the pores of the composite. This aids in the reduction of the diffusion resistance for CO₂ as well as increases

accessibility to amine sites [39]. However, on further increasing the amine loading to 50 wt%, the pore blockage results in weakening of physical adsorption. The amine molecules are unable to develop sufficient chemical adsorption force, which can exceed the combined physico-chemical forces to adsorb the CO₂ molecules. Hence, the adsorption drastically reduced to 0.65 mmol/g. MIL/SBA/PEI-25 incorporating 25 wt% of PEI showed a maximum adsorption capacity of 3.2 mmol/g, and hence it was optimized for further studies. Based on the above observations, the various stages of CO2 adsorption on the composite involves: i) Diffusion of CO₂ molecules from gas phase to the adsorbent surface, ii) Diffusion of CO₂ molecules from the adsorbent surface to the pore which is indicative of physisorption, iii) Chemical reaction of CO₂ with adsorbent resulting in production of carbon-containing compounds which is indicative of chemisorption, iv) Adsorption saturation due to pore blockage. The round pellets of MIL/SBA/PEI-25, formed using PMMA as a binder, showed around 9 % reduction in their adsorption capacity (2.9

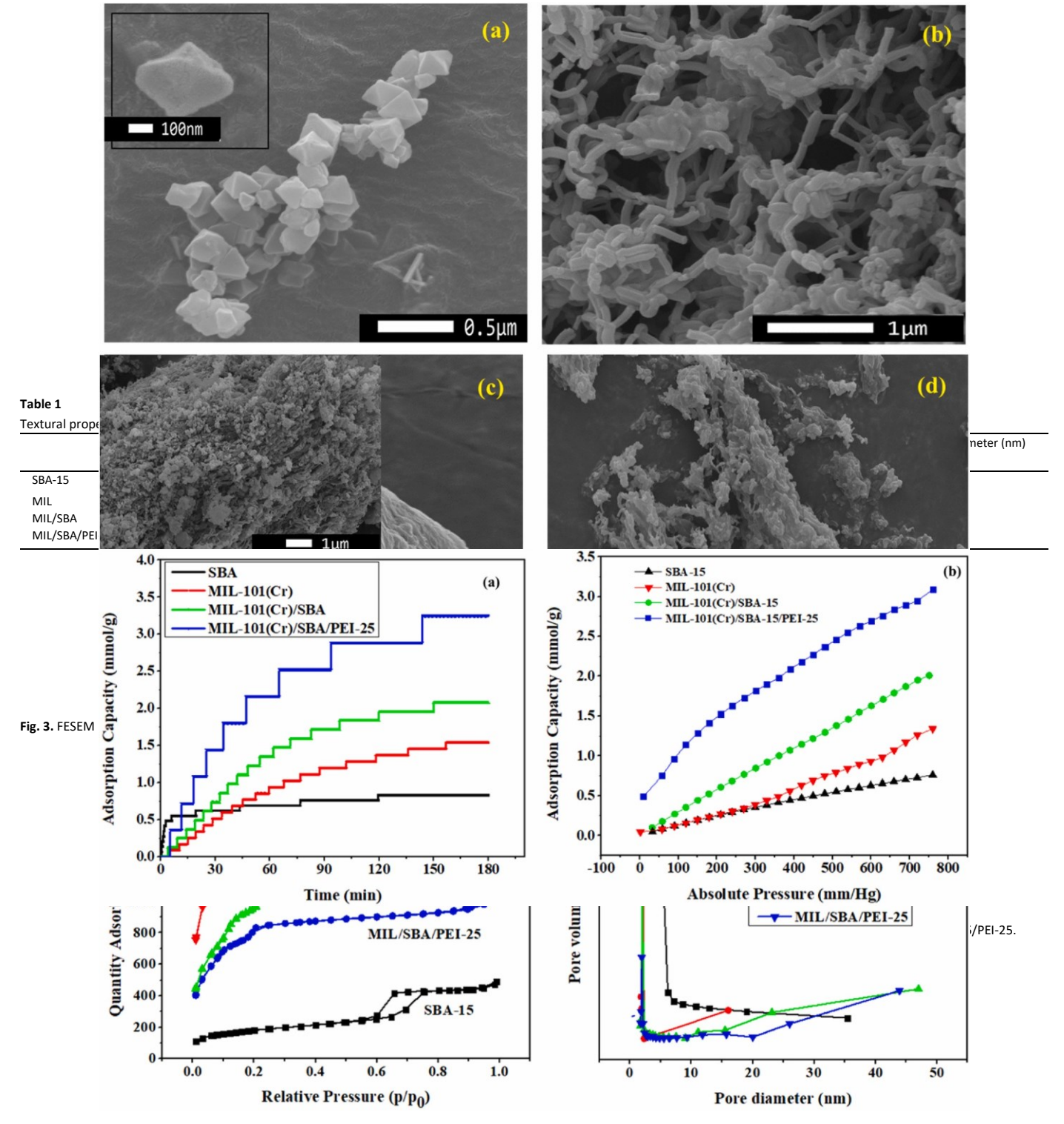


Fig. 4. (a) N2 adsorption-desorption isotherms and(b) BJH pore size distributions of SBA-15, MIL-101(Cr), MIL-101(Cr)/SBA-15, MIL-101(Cr)/SBA-15,

mmol/g) (Fig. S5). The favorable permeance of CO_2 in PMMA retained the adsorption property of the composite. Hence, this MOF shaping strategy using PMMA binder proved to be suitable resulting in minimum alteration of gas adsorption property. Fig. S6 represents the mean CO_2 uptake capacity of the studied adsorbents, with error bars indicating the range between the maximum and minimum values observed within each set of triplicates.

The composite MIL/SBA/PEI-25 also exhibited excellent adsorption of 400 ppm CO $_2$ (Fig. S7). The adsorption capacity was found to be 1.6 mmol/g for 180 min of adsorption at 30 °C and 1 bar. The reduction in driving force, i.e., CO $_2$ concentration, resulted in a decrease in the adsorption capacity. The CO $_2$ adsorption from the dilute stream was very rapid within the initial period of 20 min. Pseudo-equilibrium was obtained approximately after 110 min contact time.

The CO_2/N_2 selectivity has been estimated using gas mixture of 0.15 bar CO_2 and 0.75 bar N_2 . The N_2 adsorption of MIL/SBA is higher than MIL/SBA/PEI-25 due to its larger surface area (Fig. S8). The N_2 adsorption capacity of both composites is lower than their CO_2 adsorption capacity. This can be ascribed to the reduction in the adsorbate-adsorbent electrostatic interaction [30]. The CO_2/N_2 selectivity decreases with increasing pressure and reaches as high as 101 for the MIL/SBA/PEI-25. Increased selectivity indicates preferential adsorption of CO_2 in a binary gas mixture of CO_2 and N_2 .

3.2.1. Adsorption isotherm

The interaction between the optimized adsorbent (MIL/SBA/PEI-25) and adsorbate (CO₂) was studied by performing the gravimetric and volumetric adsorption at three different temperatures (Fig. S9). The adsorption capacity decreased with an increase in temperature. The data were well fitted using the single site Langmuir, Sips, and Toth Adsorption Isotherm (Fig. S10), as evidenced by the correlation co-efficient (R²), and the parameters have been displayed in Table S2. All the isotherms provide a good fit to the adsorption data based on their R² values. Langmuir Isotherm indicates the dominancy of physical adsorption and hence, facile desorption of CO₂ from the adsorbent surface. The bA in Sips and Toth isotherms represents the adsorption affinity. The values of bA were found to increase with decreasing adsorption temperature representing better adsorption at lower temperature. The maximum Langmuir adsorption capacity was found to be 5.9 mmol/g.

The heat of adsorption (Q_{ist}) determines the strength of adsorbent-adsorbate interaction. Q_{ist} at a certain CO_2 loading has been calculated from the slope of ln P vs. 1/T (Fig. S11). MIL/SBA/PEI-25 displayed a slight change of Q_{ist} with CO_2 uptake, implying surface homogeneity and uniform adsorption [40]. Q_{ist} reduced from 52 kJ/mol to 45 kJ/mol upon increased CO_2 adsorption from 0.1 mmol/g to 1 mmol/g (Fig. S12). The range of the isosteric enthalpy as obtained indicates moderate strength of CO_2 binding on the adsorbent surface [41]. This concludes efficient desorption of CO_2 indicating facile adsorbent regeneration. Adsorbent regeneration could be achieved via pressure or temperature swing desorption.

3.2.2. Adsorption kinetics

The kinetic study for adsorption was conducted using TGA. The adsorption data of MIL, MIL/SBA-15, and MIL/SBA-15/PEI-25 were well-fitted to the pseudo-second-order kinetic model (Fig. S13), and the parameters are presented in Table S3.

. The kinetic model describes a relation between the rate of adsorption and the active sites on the adsorbent. $Q_{\rm e}$ of MIL/SBA-15/PEI- 25 was found to be 3.5 mmol/g, which is almost similar to the experimental equilibrium adsorption capacity. Additionally, the R^2 of 0.95 suggests a good fit of the data to the pseudo-second-order kinetic model. The rate constant for MIL/SBA-15/PEI-25 was found to be 0.003 g/ mmol/min, which is higher than the other synthesized materials. The presence of SBA-15 in the MOF framework enhanced the CO_2 adsorption rate as compared to solely amine-impregnated MIL-101 (K = 0.002 g/ mmol/min) [42]. This highihhts the significance of SBA-15 incorporation in the MOF framework.

3.2.3. Reusability studies

An important aspect of a novel composite is its reusability. The composite MIL/SBA-15/PEI-25 displayed around 10 % reduction in adsorption capacity after ten cycles of reuse and regeneration (Fig. 6a), with good adsorbent stability. The reduction in adsorption efficiency was maximum at 3 cycles, after which it almost stabilized. The FTIR and FESEM of the adsorbent after reuse

occurred at a much higher temperature of 348 K [43]. MIL-101 (Cr)-PEI-70 showed slightly higher CO_2 adsorption at

Table 2Adsorption capacity of reported MOFs and mesoporous materials.

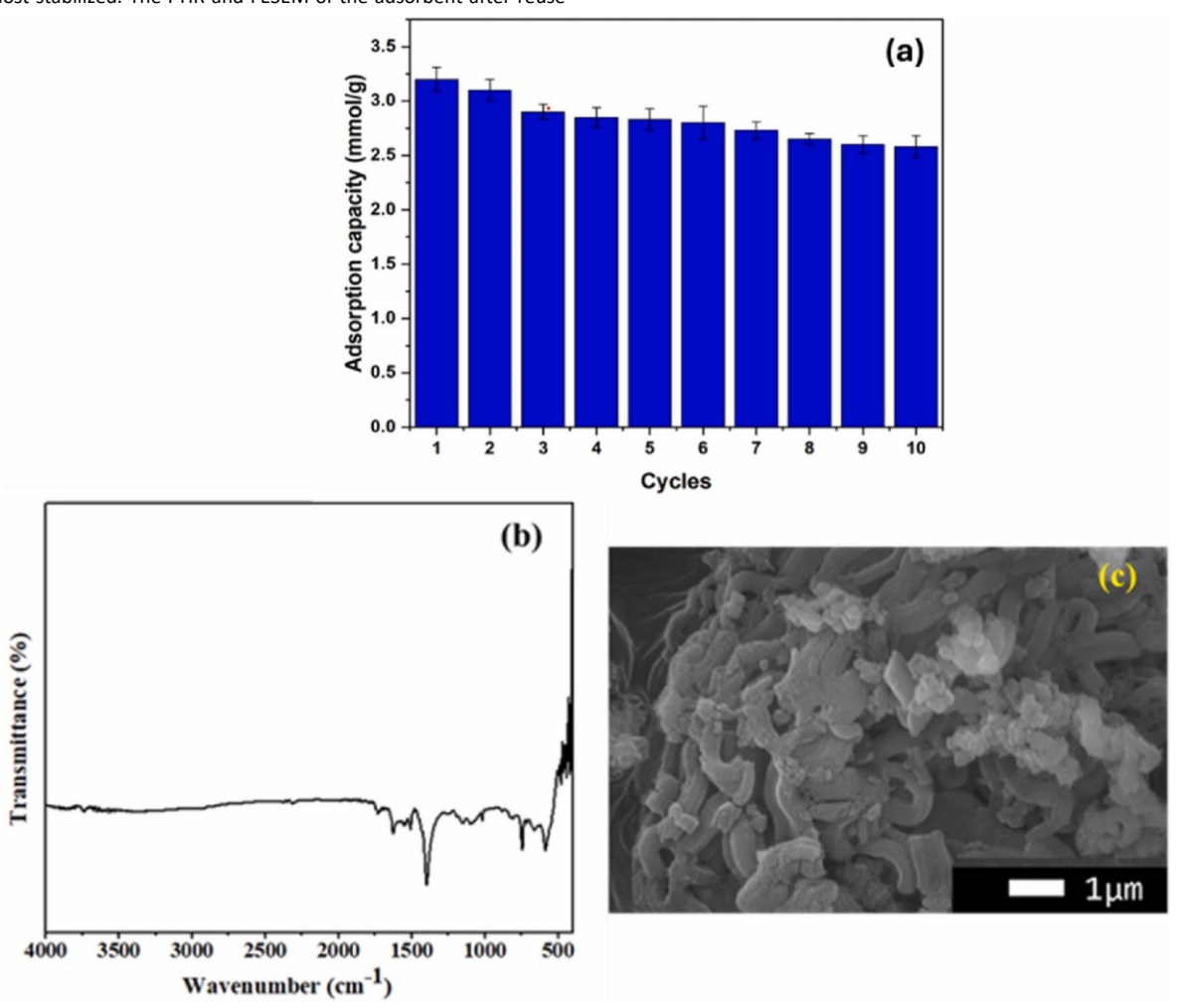


Fig. 6. (a) Adsorption capacity of MIL-101(Cr)/SBA-15/PEI-25 after reuse measured by TGA; (b) FTIR; (c) FESEM of reused MIL-101(Cr)/SBA-15/PEI-25.

Adsorbent	Condition	Adsorption capacity (mmol/g)	Method	Desorption conditions	Reference
MIL-100 (Fe)/DETA	298 K, 1 bar	1.82	Volumetric	75 °C, 1 h, He flow	[42]
MIL-101 (Cr)-PEI-70	348 K, 1 bar	3.8	Volumetric	120 °C, 2 h, vacuum	[15]
MIL-101 (Cr)	348 K	0.80	Gravimetric	150 °C, vacuum, 6 h	[44]
Zn/Co ZIF/PEI	298 K, 1 bar	1.82	Volumetric	110 °C	[45]
MOF-177/DETA	298 K, 1 bar	2.83	Gravimetric	100 °C, 40 min	[39]
ZIF-8/PEI	338 K, 1 bar	1.61	Fixed-bed breakthrough	_	[46]
PEI/MCM-41	348 K	3.1	Fixed bed	_	[43]
PEI/nanoporous carbon	348 K	1.09	Gravimetric	100 °C, 30 min, N₂ flow	[47]
PEI/mesoporous alumina	348 K	2.72	Gravimetric	100–200 °C, He flow	[48]
PEI/SWCNT	348 K	1.77	Gravimetric		[49]
MIL-101(Cr)/SBA-15/PEI	303 K, 1 bar	3.2 Q _{max} =	Gravimetric and Volumetric	65 °C, 2 h, N₂ flow	This study
		5.9			

are displayed in Fig. 6b and c, respectively. The structural and morphological properties are retained, implying adsorbent stability and reversibility of adsorption. This signifies that MIL/SBA-15/PEI-25 can be efficiently regenerated under thermal treatment at atmospheric pressure conditions.

The adsoption and desorption efficiency of the synthesized composite has been compared with similar materials, such as MOFs and mesoporous compounds, shown in Table 2. The adsorption of the tabulated composites were performed at atmospheric pressure, similar to our study. Although PEI/MCM-41 showed comparable adsorption capacity, the adsorption

348 K compared to the current study. However, higher loading of amine (70 wt%) led to a much higher desorption temperature of 120 °C. In contrast, MIL-101(Cr)/SBA-15/PEI-25 composite showed promising results at low amine loading of 25 wt%, thereby efficiently desorbing at a much lower temperature of 65 °C. Low regeneration temperature leads to lower energy consumption making the dsoprtion processs environmental-friendly.

4. Conclusions

5. The synergistic interplay of meso and macro porosity of SBA-15 incorporated MIL-101(Cr) in amalgamation with impregnated amines, acting as Lewis bases, can be used to play an important role in CO₂ capture. In summary, a cylindrical composite containing PEI- impregnated SBA incorporated MIL-101(Cr) was synthesized via an in-situ hydrothermal process. While PEI can bind to SBA-15 via hydrogen bond formation, coordinate bonding is responsible between the amine and Lewis acid sites in the MOF. SBA-15 influenced the growth and crystallization of the MOF i.e., MIL-101(Cr), resulting in increased mesopore volume of the composite, making them more suitable for CO₂ capture. The Lewis acid-base interaction between CO2 and unsaturated Cr(III) metal centers in the MOF resulted in 1.3 mmol/g of CO₂ adsorption at 303 K, 1 bar. Incorpration of SBA-15 endowed the composite with increased mesopore volume from 0.65 cm³/g to 1.62 cm³/g. This enhanced the CO₂ mass transfer rate and its adsorption to 2.1 mmol/g for MIL-101(Cr)/SBA-15. Additionally, the SBA-15 particle size drastically reduced from a few microns to a nanometer in the case of the composite, thus exposing more active adsorption sites. Furthermore, amine groups in PEI increased chemisorption due to carbamate formation. The maximum adsorption capacity for pure CO₂, as estimated from the Langmuir isotherm fit, was found to be 5.9 mmol/g, and the reaction was exothermic in nature. Markedly, low regerneration temperature of 65 °C indicates energy efficiency of the process compared to various reported adsorbent. The composite exhibited good stability for ten cycles of reuse and regeneration. In summary, the current study delineates the role of hierarchical porous adsorbents for capturing CO₂ from concentrated as well as dilute gas streams at ambient conditions.

CRediT authorship contribution statement

Debarati Mukherjee: Writing – original draft, Validation, Methodology, Investigation, Conceptualization. Saif Hassan: Writing – original draft, Methodology, Investigation. Juvairia Shajahan: Investigation. Aleksandrs Prokofjevs: Writing – review & editing, Resources. Debasish Kuila: Writing – review & editing, Supervision, Resources, Conceptualization.

Declaration of competing interest

The authors declare that they have no known competing financial interests or personal relationships that could have appeared to influence the work reported in this paper.

Data availability

Data will be made available on request.

Acknowledgments

The authors acknowledge the funding received from DOE-BES (Award Number: DE SC0022230), NSF-CREST (Award Number: DE SC0022230), NSF-CREST (Award Number: 1736173), and NSF-SENIC (Award Number: ECCS-2025462). The authors thank Dr. Shima Masoumi for her help with the XRD analysis. We gratefully acknowledge the help received from Dr. Kyle Nowlin for FETEM and FESEM studies at the Joint School of Nanoscience and Nanoengineering.

Appendix A. Supplementary data

Supplementary data to this article can be found online at https://doi.org/10.1016/j.matchemphys.2024.129533.

References

 J. Wang, J. Yang, R. Krishna, T. Yang, S. Deng, A Versatile Synthesis of Metal- Organic Framework-Derived Porous Carbons for CO 2 Capture and Gas Separation, 2016.

- [2] G. Rim, F. Kong, M. Song, C. Rosu, P. Priyadarshini, R.P. Lively, C.W. Jones, Sub- ambient temperature direct air capture of CO2using amine-impregnated MIL-101 (Cr) enables ambient temperature CO2Recovery, JACS Au 2 (2022) 380–393, https://doi.org/10.1021/jacsau.1c00414.
- B.L. Salvi, S. Jindal, Recent developments and challenges ahead in carbon capture and sequestration technologies, SN Appl. Sci. (2019), https://doi.org/10.1007/ s42452-019-0908-2
- [4] D.Y.C. Leung, G. Caramanna, M.M. Maroto-Valer, An overview of current status of carbon dioxide capture and storage technologies, Renew. Sustain. Energy Rev. (2014), https://doi.org/10.1016/j.rser.2014.07.093.
- [5] J. Wang, L. Huang, R. Yang, Z. Zhang, J. Wu, Y. Gao, Q. Wang, D. O'hare, Z. Zhong, Recent advances in solid sorbents for CO 2 capture and new development trends, Energy Environ. Sci. 7 (11) (2014) 3478–3518, https://doi.org/10.1039/C4EE01647E.
- [6] B. Guo, L. Chang, K. Xiel, mMv adsorption of carbon dioxide on activated carbon, elsevia.comilmxie/jngc Journal of Natural Gas Chemistry. (2006).
- [7] M. Cinke, J. Li, C.W. Bauschlicher, A. Ricca, M. Meyyappan, CO2 adsorption in single-walled carbon nanotubes, Chem. Phys. Lett. 376 (2003) 761–766, https://doi.org/10.1016/S0009-2614(03)01124-2.
- [8] Y. Cho, Ji Yun Lee, A.D. Bokare, S.B. Kwon, D.S. Park, W.S. Jung, J.S. Choi, Y. M. Yang, Ju Yeol Lee, W. Choi, LiOH-embedded zeolite for carbon dioxide capture under ambient conditions, J. Ind. Eng. Chem. 22 (2015) 350–356, https://doi.org/ 10.1016/j.jiec.2014.07.030.
- [9] Y. Bang, S.J. Han, S. Kwon, V. Hiremath, I.K. Song, J.G. Seo, High temperature carbon dioxide capture on Nano-structured MGO-AL2O3 and CAO-AL2O3 adsorbents: an experimental and theoretical study, J. Nanosci. Nanotechnol. 14 (2014) 8531–8538, https://doi.org/10.1166/jnn.2014.9954.
- [10] L. Zhao, Y. Chen, B. Wang, C. Sun, S. Chakraborty, K. Ramasubramanian, P. K. Dutta, W.S.W. Ho, Multilayer polymer/zeolite Y composite membrane structure for CO2 capture from flue gas, J. Membr. Sci. 498 (2016) 1–13, https://doi.org/10.1016/j.memsci.2015.10.006.
- [11] Z. Zhang, Z.-Z. Yao, S. Xiang, B. Chen, Perspective of microporous metal—organic frameworks for CO ₂ capture and separation, Energy Environ. Sci. 7 (2014) 2868, https://doi.org/10.1039/C4EE00143E.
- [12] P. Das, D. Mukherjee, B. Mandal, S. Gumma, Engineering of interfacial energy bands for synthesis of photoluminescent 0D/2D coupled MOF heterostructure with enhanced selectivity toward the proton-exchange membrane, ACS Appl. Mater. Interfaces 13 (2021) 29619–29630, https://doi.org/10.1021/acsami.1c06152.
- [13] Y.B. Huang, J. Liang, X.S. Wang, R. Cao, Multifunctional metal-organic framework catalysts: synergistic catalysis and tandem reactions, Chem. Soc. Rev. (2017), https://doi.org/10.1039/c6cs00250a.
- [14] J. Li, Xiangxue Wang, G. Zhao, C. Chen, Z. Chai, A. Alsaedi, T. Hayat, Xiangke Wang, Metalorganic framework-based materials: superior adsorbents for the capture of toxic and radioactive metal ions, Chem. Soc. Rev. (2018), https://doi.org/10.1039/c7cs00543a.
- [15] S. Mutyala, M. Jonnalagadda, H. Mitta, R. Gundeboyina, CO2 capture and adsorption kinetic study of amine-modified MIL-101 (Cr), Chem. Eng. Res. Des. 143 (2019) 241–248, https://doi.org/10.1016/j.cherd.2019.01.020.
- [16] C. Ferey, C. Mellot-Draznieks, C. Serre, F. Millange, J. Dutour, S. Surbl' e, 'I. Margiolaki, Chemistry: a chromium terephthalate-based solid with unusually large pore volumes and surface area, Science 309 (2005) 2040–2042, https://doi.org/10.1126/science.1116275.1979.
- [17] Y. Kim, T. Yang, G. Yun, M.B. Ghasemian, J. Koo, E. Lee, S.J. Cho, K. Kim, Hydrolytic transformation of microporous metal—organic frameworks to hierarchical micro- and mesoporous MOFs, Angew. Chem. 127 (2015) 13471–13476, https://doi.org/10.1002/ange.201506391.
- [18] S. Liu, L. Sun, F. Xu, J. Zhang, C. Jiao, F. Li, Z. Li, S. Wang, Z. Wang, X. Jiang, H. Zhou, L. Yang, C. Schick, Nanosized Cu-MOFs induced by graphene oxide and enhanced gas storage capacity, Energy Environ. Sci. 6 (2013) 818–823, https://doi.org/10.1039/c3ee23421e.
- [19] N.E. Tari, A. Tadjarodi, J. Tamnanloo, S. Fatemi, One pot microwave synthesis of MCM-41/Cu based MOF composite with improved CO2 adsorption and selectivity, Microporous Mesoporous Mater. 231 (2016) 154–162, https://doi.org/10.1016/j.micromeso.2016.05.027.
- [20] G. Zhou, S. Yang, Y. Tian, Y. Liu, Z. Liu, X. Dong, Adsorption application of tetraethylenepentamine (TEPA) modified SBA-15@MIL-101(Cr) in carbon capture and storage (CCS), Microporous Mesoporous Mater. 344 (2022), https://doi.org/ 10.1016/j.micromeso.2022.112232.
- [21] A. Chakraborty, T.K. Maji, Mg-MOF-74@SBA-15 hybrids: synthesis, characterization, and adsorption properties, Apl. Mater. 2 (2014), https://doi.org/ 10.1063/1.4902816.
- [22] C. Chen, H. Wang, Y. Chen, X. Wei, W. Zou, H. Wan, L. Dong, G. Guan, Layer-by- layer self-assembly of hierarchical flower-like HKUST-1-based composite over amino-tethered SBA-15 with synergistic enhancement for CO2 capture, Chem. Eng. J. 413 (2021), https://doi.org/10.1016/j.cej.2020.127396.
- [23] F. Martínez, R. Sanz, G. Orcajo, D. Briones, V. Yangüez, Amino-impregnated MOF materials for CO2 capture at post-combustion conditions, Chem. Eng. Sci. 142 (2016) 55–61.
- [24] K. Pirzadeh, A.A. Ghoreyshi, S. Rohani, M. Rahimnejad, Strong influence of amine grafting on MIL-101 (Cr) metal—organic framework with exceptional CO2/N2 selectivity, Ind. Eng. Chem. Res. 59 (1) (2019) 366–378.
- [25] P. Muchan, C. Saiwan, M. Nithitanakul, Investigation of adsorption/desorption performance by aminopropyltriethoxysilane grafted onto different mesoporous silica for post-combustion CO2 capture, Clean Energy 4 (2) (2020) 120–131. [26] A. Mallick, G. Mouchaham, P.M. Bhatt, W. Liang, Y. Belmabkhout, K. Adil, A. Jamal, M. Eddaoudi,

- Advances in shaping of metal-organic frameworks for CO2 capture: understanding the effect of rubbery and glassy polymeric binders, Ind.
 Eng. Chem. Res. 57 (2018) 16897–16902, https://doi.org/10.1021/acs.iecr.8b03937.
- [27] H. Eslami, M. Kesik, H.A. Karimi-Varzaneh, F. Müller-Plathe, Sorption and diffusion of carbon dioxide and nitrogen in poly(methyl methacrylate), J. Chem. Phys. 139 (2013), https://doi.org/10.1063/1.4821585.
- [28] L. Bromberg, Y. Diao, H. Wu, S.A. Speakman, T.A. Hatton, Chromium(III) terephthalate metal organic framework (MIL-101): Hf-free synthesis, structure, polyoxometalate composites, and catalytic properties, Chem. Mater. 24 (2012) 1664–1675, https://doi.org/10.1021/cm2034382.
- [29] J. Park, Y.S. Chae, D.W. Kang, M. Kang, J.H. Choe, S. Kim, J.Y. Kim, Y.W. Jeong, C. S. Hong, Shaping of a metal-organic framework-polymer composite and its CO2Adsorption performances from humid indoor air, ACS Appl. Mater. Interfaces 13 (2021) 25421– 25427, https://doi.org/10.1021/acsami.1c06089.
- [30] F. Gao, S. Wang, G. Chen, J. Duan, J. Dong, W. Wang, A facile approach to the fabrication of MgO@ Y composite for CO 2 capture, Adsorption 26 (2020) 701–709
- [31] S. Kalam, S.A. Abu-Khamsin, M.S. Kamal, S. Patil, Surfactant adsorption isotherms: a review, ACS Omega (2021), https://doi.org/10.1021/acsomega.1c04661.
- [32] S. Khoshhal Salestan, K. Pirzadeh, A. Rahimpour, R. Abedini, Poly (ether-block amide) thin-film membranes containing functionalized MIL-101 MOFs for efficient separation of CO2/CH4, J. Environ. Chem. Eng. 9 (2021) 105820, https://doi.org/10.1016/j.jece.2021.105820.
- [33] S. Sain, D. Ray, A. Mukhopadhyay, S. Sengupta, T. Kar, C.J. Ennis, P.K. Rahman, Synthesis and characterization of PMMA-cellulose nanocomposites by in situ polymerization technique, J. Appl. Polym. Sci. 126 (S1) (2012) E127–E134.
- [34] F. Yang, C.X. Yang, X.P. Yan, Post-synthetic modification of MIL-101(Cr) with pyridine for high-performance liquid chromatographic separation of tocopherols, Talanta 137 (2015) 136–142, https://doi.org/10.1016/j.talanta.2015.01.022.
- [35] O.K. Farha, I. Eryazici, N.C. Jeong, B.G. Hauser, C.E. Wilmer, A.A. Sarjeant, R. Q. Snurr, S.T. Nguyen, A.O. Yazaydın, J.T. Hupp, Metal-organic framework materials with ultrahigh surface areas: is the sky the limit? J. Am. Chem. Soc. 134 (36) (2012) 15016–15021.
- [36] H. Torabi, H. Eshghi, S.S. Ghodsinia, P. Sanati-Tirgan, Design and synthesis of ZnGlu MOF/SBA-16 nanocomposite, and its performance as an environmentally friendly nanocomposite for solvent-free chemical fixation of CO2 to epoxides for high-yield synthesis of cyclic carbonates, Mol. Catal. 550 (2023) 113552.
- [37] C. Chen, B. Li, L. Zhou, Z. Xia, N. Feng, J. Ding, L. Wang, H. Wan, G. Guan, Synthesis of hierarchically structured hybrid materials by controlled self-assembly of metal-organic framework with mesoporous silica for CO2 adsorption, ACS Appl. Mater. Interfaces 9 (2017) 23060–23071, https://doi.org/10.1021/acsami.7b08117.
- [38] Z. Karimi, A. Morsali, Modulated formation of metal-organic frameworks by oriented growth over mesoporous silica. https://doi.org/10.1039/b000000x, 2013.
- [39] S. Gaikwad, Y. Kim, R. Gaikwad, S. Han, Enhanced CO2capture capacity of amine-functionalized MOF-177 metal organic framework, J. Environ. Chem. Eng. 9 (2021), https://doi.org/10.1016/j.jece.2021.105523.
- [40] X. Zhou, W. Huang, J. Miao, Q. Xia, Z. Zhang, H. Wang, Z. Li, Enhanced separation performance of a novel composite material GrO@MIL-101 for CO2/CH4 binary mixture, Chem. Eng. J. 266 (2015) 339–344, https://doi.org/10.1016/j. cej.2014.12.021.
- [41] Mingzhe Sun, Qinfen Gu, Aamir Hanif, Tianqi Wang, Jin Shang, Transition metal cation-exchanged SSZ-13 zeolites for CO2 capture and separation from N2, Chem. Eng. J. 370 (2019) 1450–1458.
- [42] S. Mutyala, S.M. Yakout, S.S. Ibrahim, M. Jonnalagadda, H. Mitta, Enhancement of CO2 capture and separation of CO2/N2 using post-synthetic modified MIL-100(Fe), New J. Chem. 43 (2019) 9725–9731, https://doi.org/10.1039/c9nj02258a.
- [43] X. Ma, X. Wang, C. Song, "Molecular basket" sorbents for separation of CO 2 and H 2S from various gas streams, J. Am. Chem. Soc. 131 (2009) 5777–5783, https://doi.org/10.1021/ja8074105.
- [44] G. Zhou, S. Yang, Y. Tian, Y. Liu, Z. Liu, X. Dong, Adsorption application of tetraethylenepentamine (TEPA) modified SBA-15@MIL-101(Cr) in carbon capture and storage (CCS), Microporous Mesoporous Mater. 344 (2022), https://doi.org/ 10.1016/i.micromeso.2022.112232.
- [45] J. Cheng, N. Liu, L. Hu, Y. Li, Y. Wang, J. Zhou, Polyethyleneimine entwine thermally-treated Zn/Co zeolitic imidazolate frameworks to enhance CO2 adsorption, Chem. Eng. J. 364 (2019) 530–540, https://doi.org/10.1016/j.cej.2019.02.026.
- [46] S. Xian, F. Xu, C. Ma, Y. Wu, Q. Xia, H. Wang, Z. Li, Vapor-enhanced CO2 adsorption mechanism of composite PEI@ZIF-8 modified by polyethyleneimine for CO2/N2 separation, Chem. Eng. J. 280 (2015) 363–369, https://doi.org/10.1016/ i.cej.2015.06.042.
- [47] Z. Tang, Z. Han, G. Yang, J. Yang, Polyethylenimine loaded nanoporous carbon with ultralarge pore volume for CO 2 capture, Appl. Surf. Sci. 277 (2013) 47–52, https://doi.org/10.1016/j.apsusc.2013.03.142.
- [48] C. Chen, W.S. Ahn, CO 2 capture using mesoporous alumina prepared by a sol-gel process, Chem. Eng. J. 166 (2011) 646–651, https://doi.org/10.1016/j. cej.2010.11.038.
- [49] E.P. Dillon, C.A. Crouse, A.R. Barron, Synthesis, characterization, and carbon dioxide adsorption of covalently attached polyethyleneimine-functionalized single- wall carbon nanotubes, ACS Nano 2 (2008) 156–164, https://doi.org/10.1021/nn7002713.